CO_2 capture using highly viscous amine blends in non-porous membrane contactors

Luca Ansaloni, Ardi Hartono, Muhammad Awais, Hanna K. Knuutila, Liyuan Deng

PII: S1385-8947(18)32244-7
DOI: https://doi.org/10.1016/j.cej.2018.11.014
Reference: CEJ 20316

To appear in: *Chemical Engineering Journal*

Received Date: 15 September 2018
Revised Date: 31 October 2018
Accepted Date: 2 November 2018

Please cite this article as: L. Ansaloni, A. Hartono, M. Awais, H.K. Knuutila, L. Deng, CO_2 capture using highly viscous amine blends in non-porous membrane contactors, *Chemical Engineering Journal* (2018), doi: https://doi.org/10.1016/j.cej.2018.11.014

CO_2 capture using highly viscous amine blends in non-porous membrane contactors

Luca Ansaloni[1,*], *Ardi Hartono, Muhammad Awais, Hanna K. Knuutila, Liyuan Deng*[*]
Department of Chemical Engineering, Norwegian University of Science and Technology (NTNU), Trondheim, NO-7491, Norway

[1]Present address: SINTEF Industry, Sustainable Energy Technology, Oslo, Norway (luca.ansaloni@sintef.no)

[*]Corresponding authors:

Luca Ansaloni, Tel +47 95293867, Email: luca.ansaloni@ntnu.no
Liyuan Deng, Tel. +47 73594112, Email: liyuan.deng@ntnu.no

Keywords

Non-porous membrane contactor; CO_2 capture; Amine blends; Absorbent viscosity; Liquid boundary layer.

Highlights

- CO_2 capture in non-porous membrane contactors using new amine solvents was evaluated.
- Solvent viscosity significantly affects the performance of the system.
- The mass transfer coefficient decreases with at higher CO_2 content in the feed gas.
- Liquid flow rate has limited impact on the membrane contactor performance.
- The liquid boundary layer resistance is significant for highly viscous absorbents.

Abstract

New amine blends have shown a promising potential to reduce the energy penalty for CO_2 capture in post combustion, making the deployment of carbon capture technologies one-step closer. However, their application at the industrial scale is threaten by their high volatility. Non-porous membrane contactors offer a viable solution to properly control amine emissions from these absorbents. In the present work, the CO_2 capture performance of non-porous membrane contactors using new amine blends as liquid phase was investigated in a temperature range typical for the absorption step (25 to 60 °C). Different amine blends with promising features in terms of cycling capacity and regeneration energy requirement were selected as liquid absorbents. Thin composite membranes fabricated by coating a perfluoropolymer on the top of a porous polypropylene layer were used as the interface between the gas and the liquid. At room temperature, membrane contactors using new absorbents exhibit a lower CO_2 mass transfer coefficient compared to the benchmark (30 wt% MEA), possibly due to the high viscosity of these liquids. The modelling analysis suggests that the liquid boundary layer dominates the mass transfer resistance in the temperature range up to 40 °C, but at higher temperatures, the decrease of the solvent viscosity makes the mass transfer dominated by the membrane phase. Interestingly, the new amine blends show better performance compared to the benchmark at higher CO_2 concentrations in feed gas, highlighting a good potential to capture CO_2 from concentrated flue gas from steel/cement industry or to upgrade biogas.

Graphical Abstract

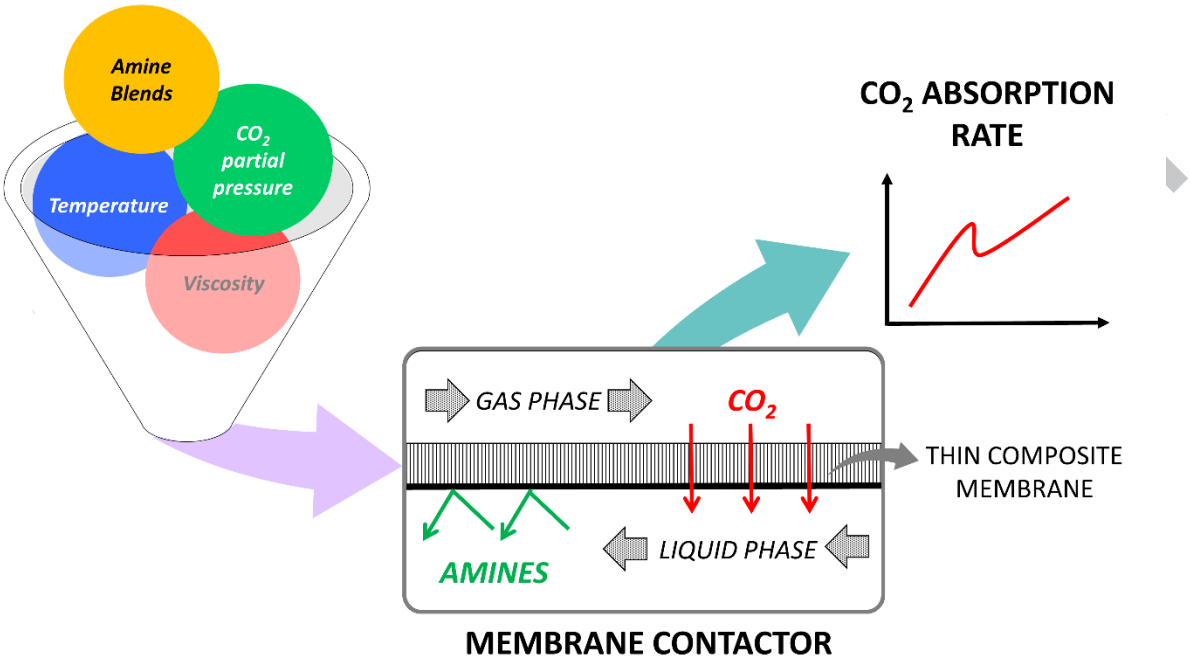

Abbreviations

3D3M = 3M DEEA 3M MAPA;

3DEAPD2M = 3M DEAPD 2M MAPA;

3HEPP2M = 3M HEPP 2M MAPA;

AF2400 = DuPont™ Teflon® AF2400 resin;

DEA-PD = 3-(diethylamino)-1,2-propanediol;

DEEA = diethylethanolamine;

HEPP = 1-(2-hydroxyethyl)pyrrolidine;

MAPA = 3-(methylamino)propylamine;

MEA = monoethanolamine;

PP = polypropylene.

1. Introduction

Upon the signing of the Paris agreement by 195 countries, actions are expected from policymakers in order to reduce the greenhouse gases emissions and hold the temperature raise of the planet within 2 °C [1]. Importance on short-term solutions becomes even more important since the 2 °C scenario does not account for regional (dry and humid lands) differences, and possibly a more drastic reduction in emissions would be required in the immediate future [2,3]. If environmental-friendly development and sustainable design of anthropogenic processes can be pursued as long-term mitigation actions, carbon capture and storage (CCS) is the most suitable short-term approach to reduce CO_2 emissions. Among available CO_2 capture solutions (amine-based absorption, solid adsorbents and membrane technology), amine-based absorption is the most mature and effective technology, especially for post-combustion applications. However, the high energy penalty associated to the regeneration step of traditional absorbents has driven a continuous research to improve the absorbent performance and make the capture step in post combustion applications more economically feasible [4].

In amine-based absorption process, the CO_2 is absorbed in the liquid phase via a chemical mechanism. For primary and secondary amines, the reaction mechanism leads to the formation of carbamate, whereas tertiary amines cannot form carbamate but simply act as proton acceptors to form bicarbonate species [5,6]. In the last decades, several types of amines have been investigated for CO_2 absorption process, aiming at improving the CO_2 absorption capacity and reducing the heat of absorption of traditional absorbents [7]. A recent publication [8] reviewed more than 130 amine-based solvents reported in literature. Although it was not possible to identify one specific solvent with superior characteristics,

several amines showed significantly better performance compared to MEA. A promising approach is offered by amine blends, which exploit the fast kinetics associated to primary/secondary amines and the larger sorption capacity and low heat of absorption related to tertiary/sterically hindered amines [5,9–11]. In particular, blends containing 3-(methylamino)propylamine (MAPA) and tertiary amines (referred also as third generation solvents) showed much better performance compared to traditional MEA-based solvents, both in terms of cyclic capacity and regeneration energy requirements [12,13]. The chemical mechanism involved behind the CO_2 absorption in this type of blended systems has been thoroughly characterized by Perinu et al. [14]. Knuutila et al. [15] reported 3 blends of MAPA with different tertiary amines (diethylethanolamine, DEEA; 1-(2-hydroxyethyl)pyrrolidine, HEPP; 3-(diethylamino)-1,2-propanediol, DEA-PD) showing 30% lower reboiler duties (2.5 – 2.6 MJ/kg CO_2) and 50% higher cyclic capacity than 30 wt% MEA. Thanks to these performances, these absorbents have a great potential to reduce the energy penalty associated with the capture step. However, their implementation at the industrial scale can be threatened by their volatility [16]: the much larger vapor pressure of the amine compounds would lead to larger amine emissions, requiring larger water wash systems and possibly causing more serious issues on surroundings of the capture plant [17].

To mitigate the negative effect of high solvent volatility, the use of thin composite membrane in membrane contactors have been proposed as a suitable solution [18,19]. Fluorinated polymers have been reported to own suitable chemical stability towards various amine-based absorbents [18] and to be characterized by a large CO_2/amine transport selectivity [19]. This latter feature is very attractive to enable the use of highly volatile CO_2 absorbents, as it can allow a substantial reduction of the amine concentration in the gas phase leaving the absorber. Advantages of membrane contactors compared to traditional

absorption columns are related to the fact that the gas/liquid interface is fixed and independent from the gas and liquid flows, to the smaller footprint due to the larger packing density and the easier scalability in view of their modularity [20]. Typically, the presence of the membrane is expected to increase the mass transfer resistance with respect to a traditional absorption column, but superior performance of membrane contactors in terms of mass transfer coefficient have also been reported [21]. In general, porous membranes [22–25] are used in membrane contactors to minimize the impact of the membrane on the mass transfer resistance, but they usually suffer from pore wetting and the consequent increase of mass transfer resistance. Nevertheless, the problem can be prevented by using thin composite membranes, since the thin dense layer in contact with the liquid prevents penetration of liquid into the pores [26–28]. The use of non-porous membrane contactors have been recently reported for both the absorption [29–31] and the desorption [32,33] step, and pilot scale investigations [34,35] have also been performed. High free volume glassy polymers (e.g., PTMSP, PIM, PMP and Teflon AF) have been used as dense coating, in order to minimize the impact of the dense coating on the CO_2 mass transfer coefficient. Despite the lower CO_2 permeability compared to PIM and PTMSP, fluorinated polymers showed the best performance in membrane contactor configuration due to their high hydrophobicity and the low liquid uptake [29], showing a promising potential in membrane contactor applications for CO_2 capture from flue gas. However, their investigation in non-porous membrane contactors has been limited to the use of MEA-based solvents, leaving the potential of different amine-based absorbents undiscovered.

In the present study, the CO_2 capture performance of different amine blend absorbents (3D3M, 3HEPP2M and 3DEAPD2M) in non-porous membrane contactors was investigated, and the results were compared with 30 wt% MEA. Thin composite membranes obtained by

coating a thin dense layer of AF2400 on the top of a porous polypropylene support were fabricated and tested in term of transport properties. To properly identify the mass transfer resistance associated to the membrane phase, both self-standing and thin composite membrane made of Teflon AF2400 were characterized by means of mixed gas permeation and membrane contactor tests. Furthermore, the effects of several operating parameters on the membrane contactor performance were investigated. The operating temperature was controlled between 23 and 60 °C, temperature range typically used in the absorption step. The CO_2 concentration in the feed gas was changed from 13 to 50 vol% (balance N_2) to study the effect of CO_2 partial pressure, maintaining the overall feed pressure close to atmospheric conditions. In view of the results observed experimentally, the influence of the liquid flow rate was also investigated, for different operating conditions. Finally, the results were analyzed by means of the resistance in series model. The assessment of each resistance (gas phase, porous support, dense layer and liquid phase) independently offers the possibility to estimate their influence on the overall transport, leading to a better understanding of the experimental results.

2. Experimental

3.1. Materials

DEEA (> 99% purity), MAPA (> 97% purity), DEAPD (> 98% purity), HEPP (> 99% purity) and monoethanolamine (MEA, > 98% purity) were purchased from Sigma Aldrich. All the solvents were used with no further purification. Deionized water was used for the preparation of the absorbent mixture. Teflon® AF2400 (T_g = 240 °C, 87 mol% dioxole content) was purchased from the Chemours Company (Wilmington, US); FC-72 was purchased from 3M (Kemi-Intressen, Sweden). Celgard LLC kindly supplied porous polypropylene (PP) support (Celgard® 2400, thickness 25 µm, porosity 41%). A certified

N_2/CO_2 gas cylinder (90 vol% N_2, 10 vol% CO_2), pure CH_4 (grade 3.5), pure N_2 (grade 5.0) and pure CO_2 (grade 5.0) were supplied by AGA Gas (AGA Gas Norge, Oslo, Norway).

3.2. Absorbent preparation and characterization

The amine aqueous mixtures were prepared by pouring a calibrated amount of amines and DI water on a rounded flask. In the case of the amine blends, the molarity of the different amines was chosen based on the performance obtained in terms of cyclic capacity and regeneration energy requirements, according to literature [15]. The molar concentration of the different components for each amine mixture is reported in Table 1.

The prepared liquid absorbents were investigated in terms of viscosity by using a rheometer (Physica MCR100, Anton Paar) with a double gap geometry in a temperature range from 25 to 80 °C.

Table 1 – Molar fraction (x) of the amine blends used in the study as liquid absorbents.

	x_{H2O}	x_{MEA}	x_{MAPA}	x_{DEEA}	x_{DEAPD}	x_{HEPP}
30% MEA	0.89	0.11	-	-	-	-
3D3M	0.74	-	0.13	0.13	-	-
3DEAPD2M	0.80	-	0.08	-	0.12	-
3HEPP2M	0.83	-	0.07	-	-	0.10

3.3. Membrane preparation

AF2400 flat-sheet samples were prepared as both self-standing films and thin composite membranes and were investigated by means of gas permeation and membrane contactor tests. The choice of AF2400 was dictated by its superior stability towards amines, as demonstrated in literature [18]. The self-supported AF2400 samples were prepared via solvent evaporation method by dropping a calibrated amount of solution (1 wt% of polymer

in FC-72) on a round petri dish. For gas separation tests, membrane with different thickness have been prepared. The thin composite membrane was fabricated by dip-coating technique. The porous PP membrane sheet was attached on a flat glass using an aluminum tape, immerged in a glass container filled with 1 wt% AF2400 solution in FC-72 and allowed to rest in a vertical position. The procedure was repeated two consecutive times, flipping the coating glass of 180° to ensure a homogenous coating layer. Both types of membrane were cured at 90 °C under vacuum conditions for 24h in order to completely remove the solvent. In the case of the self-standing films, the thickness was determined using a micrometer (Mituyoto Digimatic Indicator ID-H). For the thin composite membrane, the morphology was analyzed by means of a Scanning Electron Microscope (TM3030 tabletop microscope, Hitachi High Technologies America, Inc.). Figure 1 shows an SEM image of the prepared membrane. Different membranes have been prepared for gas permeation and membrane contactor tests, but the thickness of the dense coating layer has been found to be reproducible and corresponding to 1.7 ± 0.3 µm.

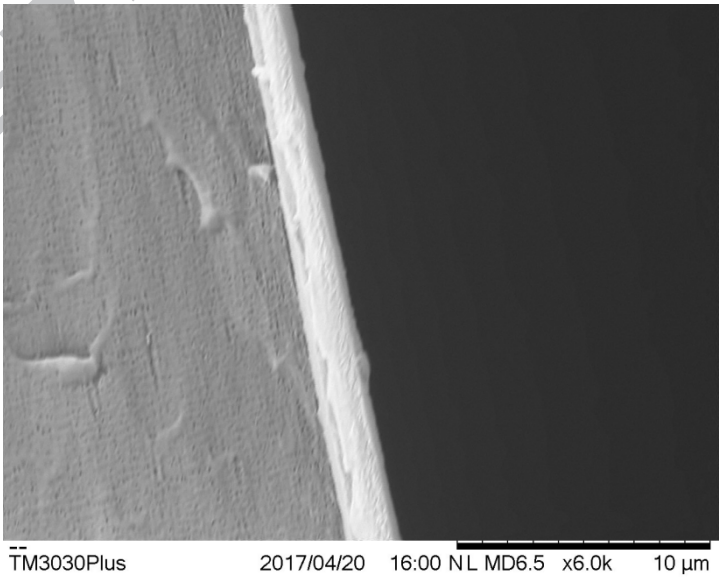

Figure 1 – Cross sectional image of the thin composite membrane, with the AF2400 coating (white layer) on the top of the porous support (light gray layer).

3.4. Gas permeation and membrane contactor tests

The gas transport properties of the fabricated membranes have been investigated by means of gas permeation experiments performed using a mixed gas permeation equipment [36]. Details of the apparatus and of the experimental conditions have been reported elsewhere [19]. In this study, a membrane cell with a permeating area of 2.2 cm^2 was used. Furthermore, the flow rates were set to 400 and 100 ml/min for the feed and sweep gas respectively. The sweep flow rate allowed to maintain a stage-cut below 4%. A calibrated gas mixture (CO_2/N_2 10/90 v/v) was used as feed gas, whereas CH_4 was used as the sweep gas. Feed stream with different CO_2 concentrations were obtained by mixing the CO_2/N_2 mixture with pure CO_2 by means of mass flow controllers and GC analysis. The pressures were kept constant at 1.4 bar for the feed side and at 1.05 bar the sweep side.

To study the capture performance of the different absorbents, membrane contactor tests were performed using the rig reported in Figure 2. A similar version was previously reported [37]. The membrane was placed in the sample holder (Fig. S1, Supporting Information), with the dense layer placed upwards and contacting the liquid phase. The interface area is 27.8 cm^2. The gas and liquid phase were flown counter currently. The feed gas mixture is created by controlled mixing of pure gases through mass flow controllers (El-Flow series, Bronkhorst, The Netherlands). The CO_2 concentration in the gas phase is detected by means of an IR-based gas analyzer (Rosemount™ X-Stream Emerson, Germany) and the gas flow rate is measured by means of a bubble flow meter placed downstream to it. To protect the CO_2 analyzer from amines or water vapors, an acid trap (0.1 M H_2SO_4) and a condenser are placed on the gas line (Fig. 2). The output gas line exiting the oven (until the acid trap) was permanently heated up to 70 °C to prevent possible condensation in the tube when the system was operated a temperature higher than room temperature.

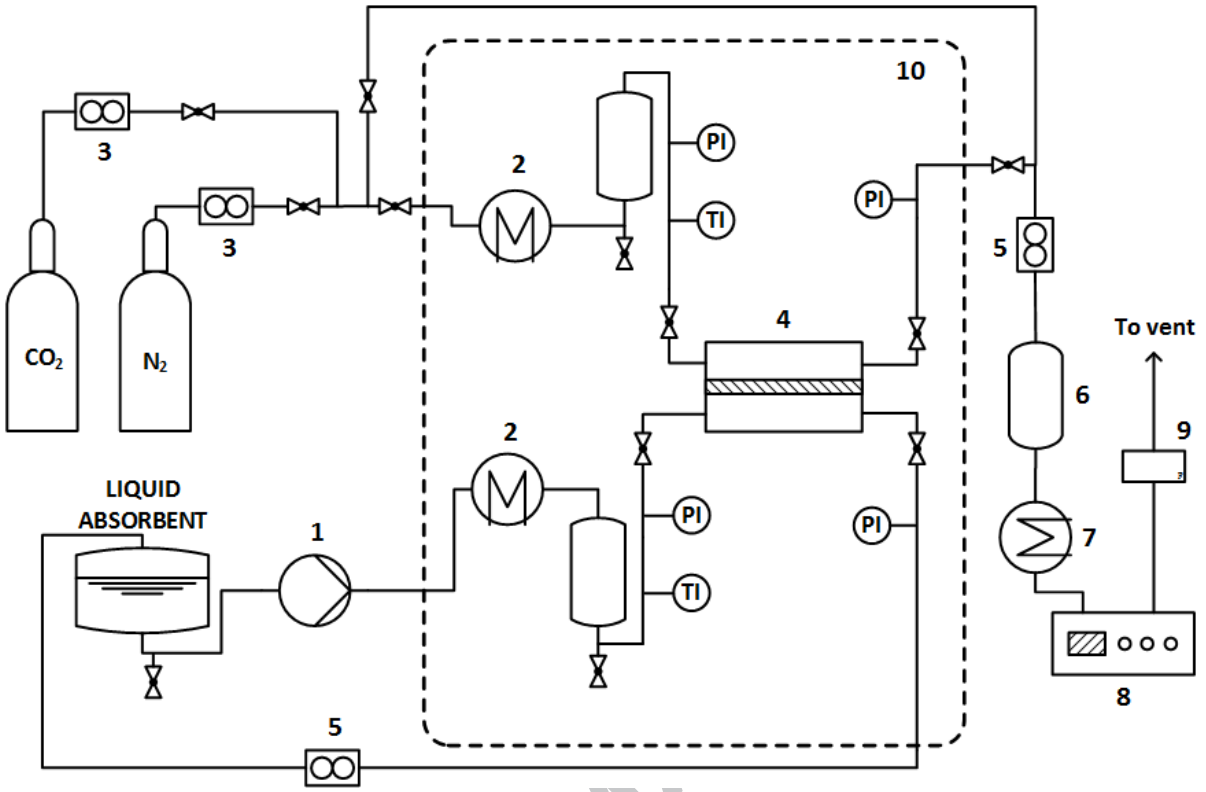

Figure 2 – Membrane contactor rig (1: liquid pump; 2: heating coil; 3: mass flow controllers; 4: membrane module; 5: back pressure regulator; 6: acid trap; 7: condenser; 8: CO_2 analyzer; 9: bubble flow meter; 10: heated cabinet; PI: pressure sensor; TI: temperature sensor).

Initially, a feed gas with a certain CO_2 concentration was created and the gas composition was measured by bypassing the membrane module. Simultaneously, the liquid is pumped through the membrane module using a magnetic gear pump (GA Series, Micropump, Labinett AB, Sweden). To start the experiment, the gaseous stream was sent to the membrane module, while monitoring the CO_2 concentration over time. Within a few minutes the steady state conditions (i.e., constant CO_2 concentration profile in the gas phase) were achieved, and the CO_2 flux per unit area (N_{CO2}, mol m^{-2} s^{-1}) was calculated according to Equation 1:

$$N_{CO2} = \frac{(Y_{CO2,in} - Y_{CO2,out}) \cdot G}{A} = K_{ov,exp} \cdot \Delta C_{CO2,\,LM} \qquad (1)$$

where $Y_{CO2,in}$ and $Y_{CO2,out}$ are the molar ratio of CO_2 in the inlet and outlet of the membrane cell, respectively, G is the gas flow rate (mol/s), and A is the permeating area

(m^2). The mass transfer coefficient (K_{exp}) can be then calculated according to:

$$K_{ov,exp} = {}^{N_{CO2}}/_{\Delta C_{CO2,\,LM}} \quad (2)$$

where $\Delta C_{CO2,\,LM}$ is the logarithmic mean of the CO_2 concentration difference between the inlet and the outlet of the membrane module.

The flow rates were investigated ranged from 250 to 350 ml/min and from 50 to 100 ml/min for the gas and the liquid phase, respectively. For both liquid and gas sides, the pressure is regulated by backpressure regulators. Both the gas and liquid pressures were kept slightly over the atmospheric pressure, at a value of about 1.1 to 1.2 bar. All the process parameters are logged using an in-house designed LabView interface. The CO_2 loading was measured by Total Inorganic Carbon (TIC) analyzer. During all experiments, the CO_2 loading of the absorbent is maintained below 0.1 $mol/mol_{amine\text{-}group}$, so that the CO_2 partial pressure in equilibrium with the liquid phase was below 0.5 kPa (i.e., the CO_2 driving force is maximized and negligibly affected).

3. Modelling

In a membrane contactor, the CO_2 mass transfer can be described using the resistance in series model, which distinguishes between each contribution from the different phases (gas, membrane and liquid phase) to the overall resistance [20]. The overall mass transfer coefficient (K_{ov}) is described as:

$$\frac{1}{K_{ov}} = \frac{1}{k_g} + \frac{1}{k_m} + \frac{1}{m\,E\,k_l} \quad (3)$$

where k_g, k_m and k_l are the gas, the membrane and the liquid mass transfer coefficient, respectively, m is the partitioning coefficient and E is the enhancement factor associated to the chemical reaction.

The mass transfer coefficient of the membrane phase is described as the contribution of the

porous support (k_{ps}) and of the dense layer (k_{dl}) according to the following formulation:

$$\frac{1}{k_m} = \frac{1}{k_{ps}} + \frac{1}{k_{dl}} = \frac{\delta_{ps}\,\tau}{D_{CO_2,g}\,\varepsilon} + \frac{\delta_{dl}\,v_m}{P\,R\,T} \quad (4)$$

where δ_{ps} and δ_{dl} are the thickness of the porous support and of the dense layer, respectively, τ and ε are the tortuosity and the porosity of the porous support, v_m is the molar volume, P is the CO_2 permeability of the dense layer, R is the gas constant and T is the operating temperature. The tortuosity is calculated as function of the porosity [38], according to the following equation:

$$\tau = \frac{(2-\varepsilon)^2}{\varepsilon} \quad (5)$$

Further details about the modelling are reported in the Appendix.

4. Results and discussion

3.1. Characterization of the absorbents' viscosity

Figure 3 displays the viscosity of the unloaded amine-based absorbents used in the present study as a function of temperature. As expected, the increase of temperature determined a drop in viscosity for all the absorbents. In the case of the MEA-based solvent, the value ranged between 2.9 and 0.9 mPa·s, in line with literature data in the entire T range investigated (as shown by the black line in Fig. 3). However, due to the larger amine concentration and the amine nature, the three third generation solvents showed higher viscosity, 6 to 9 times larger than the one obtained for 30% MEA. The increase of the operating temperature determined a sharper viscosity decrease for the amine blends, but differences of about three folds were still observed in the high temperature range compared to the benchmark.

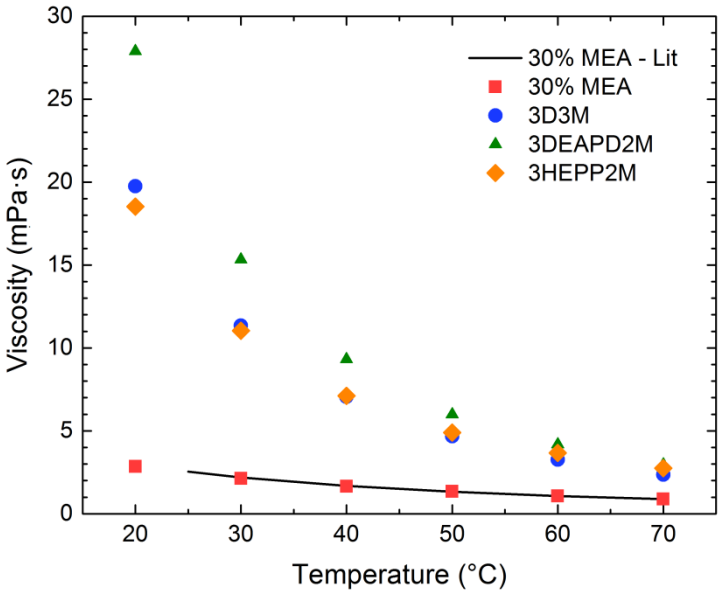

Figure 3 – Viscosity of unloaded liquid absorbents as a function of temperature. Literature data for 30 wt% MEA are obtained from Zhang et al [39].

3.2. Permeation properties of the membrane

Gas permeation properties of the thin composite membrane used in the membrane contactor were tested to provide data for the modelling analysis. As shown in Figure 4, the CO_2 permeability obtained for the selective layer of the thin composite membrane is different from the one observed for its thick self-standing counterpart. For the thick self-standing membrane at room temperature, the CO_2 permeability was found to be slightly above 4000 Barrer, and the increase of temperature determined a drop to 3300 and 2500 Barrer at 40 and 60 °C, respectively. On the contrary, for the composite membrane with a porous support, the CO_2 permeability of the thin AF2400 layer appears to be significantly lower: a value of only about 2000 Barrer was obtained at room temperature. The increase of the operating temperature has also resulted in a drop in the CO_2 permeability value (1680 and 1350 Barrer at 40 and 60 °C, respectively), similar to the thick membrane, although the slope appeared to be slightly reduced. By using the Arrhenius correlation, the activation energy of permeation increased from -12 to -8.8 kJ/mol.

A possible explanation can be associated to the influence of the porous support. Therefore, Eq. 4 has been used to calculate the influence of the porous support on the gas permeation through the membrane and the dotted line reported in Figure 4 shows the results. Despite the porous support is characterized by low porosity (ε = 41%), a very limited effect on the membrane performance is observed. For this reason, a series of self-standing membranes (thickness ranging from 5 to 43 μm) has been prepared and tested at room temperature conditions. The results are reported in Figure 5, where the permeability value is normalized using the one reported for the self-standing membrane (Fig. 4). The empty square differentiates the thin composite membrane (AF2400 selective layer coated on porous polypropylene) from the self-standing ones.

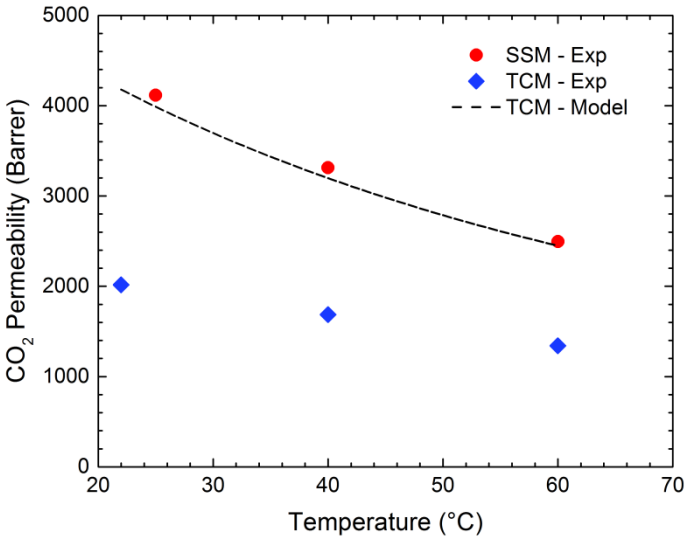

Figure 4 – CO_2 permeability of self-standing (SSM, 43 μm) and thin composite (TCM, 1.7 μm coating on porous PP) AF2400 membranes at different operating temperature. The dotted line shows the effect of the porous layer on the performance of SSM according to Eq. 4.

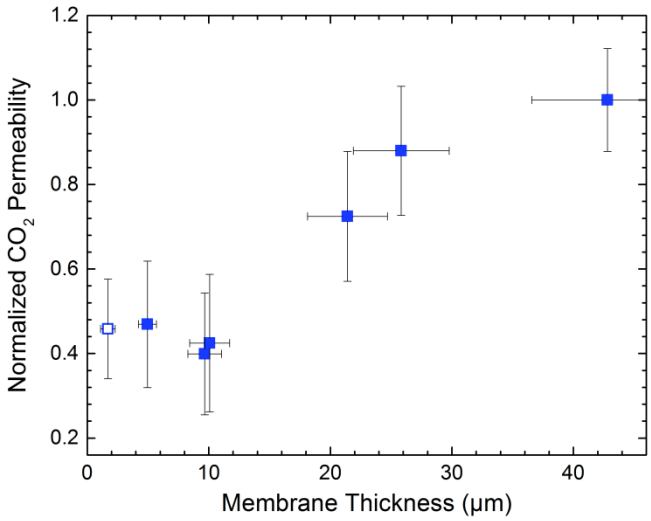

Figure 5 – Effect of membrane thickness of the CO_2 permeability of AF2400 membranes measured at room temperature.

For samples thicker than 30 μm, a CO_2 permeability value slightly above 4000 Barrer was observed, whereas for thicknesses below 15 μm the value appeared to be halved. Although the standard deviation associated to the membrane thickness generated relatively large error bars, different CO_2 permeabilities are clearly shown for thin and thick membrane. As previously mentioned, the stage cut was maintained below 4% for all the tests, limiting any influence of concentration polarization in the permeate side. A similar effect of thickness on CO_2 permeability has been already reported in literature for PDMS membranes [40], which similarly to AF2400 are characterized by high free volume. The observed effect may be attributed to surface phenomena affecting the matrix free volume, which become more dominant for thin samples compared to the bulk behavior of thick films.

3.3. Mass transfer coefficient in membrane contactor

4.3.1 Effect of operating temperature

Membrane contactor tests were performed in a temperature range typical for the absorption step (20 to 60 °C). Both self-standing and thin composite membranes with different selective layer thickness were employed in the membrane contactors for tests to

assess the impact of the membrane and the liquid phase on the overall CO_2 transport. In the first case, at room temperature, the mass transfer coefficient was found to be around 2×10^{-4} m/s and the performance appears to be limitedly influenced by the nature of the absorbent (Figure 6). By increasing the operating temperature, a decrease of the overall mass transfer coefficient was observed (1.6×10^{-4} and 1.3×10^{-4} m/s at 40 and 60 °C, respectively). As it is a thick self-standing membrane (~10 μm in thickness), it is reasonable to assume that the membrane phase dominates the resistance of the system. The negative activation energy of the permeation and the negligible effect of the nature of the absorbent clearly support this assumption.

When the thin composite membrane was used, the performances of the membrane contactor notably increased, but to a different extent depending on the type of the absorbents. In the case of 30 wt% MEA, a high mass transfer coefficient of 7.6×10^{-4} m/s was achieved at room temperature. By increasing the operating temperature from 40 to 60 °C, the mass transfer coefficient dropped from 6.3×10^{-4} to 5.1×10^{-4} m/s. Typically, the mass transfer in the liquid absorbent is expected to increase with temperature, therefore the performance drop at higher temperature observed in our test suggests that the membrane phase dominates the mass transfer. Comparison of the obtained results with literature showed that the values measured in the present study are in the same order of magnitude of the mass transfer coefficients previously reported for porous membrane contactors using similar MEA-based solvents [41]. Unfortunately, a direct comparison is not possible since 30 wt% MEA was reported to easily wet porous polypropylene [42].

When the amine blends were used, different trends were observed. At room temperature, the mass transfer coefficient appeared to be close to the performance obtained with the thick self-standing membrane, and it increased along with the operating temperature. In

addition, the performance appeared to be related to the absorbent viscosity: 3DEAPD2M, which had the highest viscosity (Fig. 3) among the three amine blends investigated in this work, showed the lowest mass transfer coefficient. On the other hand, the similar viscosity of 3D3M and 3HEPP2M (Fig. 3) resulted in similar $K_{ov,exp}$values. Differently from the benchmark, the mass transfer coefficient of the amine blends increases along with the operating temperature, reaching the performance of the benchmark at 60 °C. A possible reason for the observed phenomenon is related to the high viscosity of the amine blends compared to the benchmark solvent. Indeed, the convergence of the mass transfer coefficient values obtained for 30 wt% MEA and the different amine blends at higher temperature is similar to the one observed for the viscosity (Fig. 4). Comparable effects of absorbents viscosity on the performance of membrane contactor were observed also in the case of porous membrane contactors [43]. According to the results observed, higher operating temperatures are preferable when highly viscous solvents are used as liquid phase in non-porous membrane contactor systems as can be seen in Figure 6.

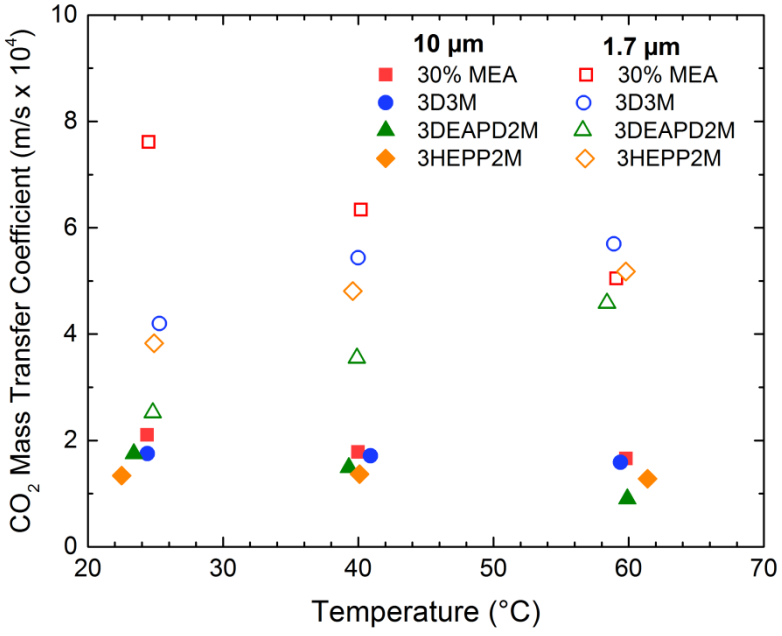

Figure 6 – Effect of operating temperature on the overall mass transfer coefficient of thick self-standing (10 µm) and thin composite (1.7 µm coating on PP) AF2400 membranes. Operating condition: liquid flow = 50 ml/min; gas flow = 250 ml/min; upstream pressure ≈ 1.1 bar; feed composition: 13 vol% CO_2 in N_2.

4.3.2 Effect of CO_2 concentration

To fully evaluate the potential of the absorbents in different applications such as post-combustion CO_2 capture from power plant or upgrade of biogas, the CO_2 concentration in the feed gas was changed from 13 to 50 vol% (balance N_2), keeping the overall pressure slightly above the atmospheric value. The three different amine blends as well as for the benchmark solvent have been used in the tests. Figure 7, 8 and 9 show the results obtained for 30% MEA, 3D3M and 3HEPP2M together with 3DEAPD2M, respectively (the CO_2 capture efficiency calculated from the experimental data is reported in the SI for all the various absorbents and operating conditions, Figure S2, S3 and S4).

In the case of 30 wt% MEA, at room temperature, the mass transfer coefficient is found to decrease at higher CO_2 concentration (Fig. 7B): the mass transfer reduced from 7.6×10^{-4} m/s to 2.2×10^{-4} m/s at 50 vol% CO_2 (overall 72% decrease). The higher CO_2 content in the feed gas determined an increase of the transmembrane flux (Fig. 7A) up to 30 vol% CO_2, followed by a plateau at higher CO_2 content. The reason for this could be related to high concentration of the CO_2 dissolved in the solvent at the membrane interface, reducing the availability of free amines at the liquid boundary layer. This indicates that, despite the presence of the dense layer coating on the porous support, at high CO_2 content in the feed gas the main resistance of the system shifted from the membrane phase to the liquid phase. The decrease of CO_2 mass transfer at higher temperature (reported in Fig. 6) is visible at all CO_2 concentrations tested as shown in Fig. 7A. The increase of CO_2 amount from 10 to 50 vol% CO_2 in the feed gas decreased the mass transfer coefficient by 73% at both 40 and 60°C. Furthermore, at all tested temperatures, the CO_2 flux reached a plateau at a CO_2 content > 30 vol%.

Different trends were observed in the case of the amine blends. Figure 8 displays the

performance measured when 3D3M was used as the CO_2 absorbent. At room temperature conditions, a drop in the mass transfer coefficient was observed at increasing the CO_2 content in the feed gas, but the extent of the variation is lower compare to 30 wt% MEA. By increasing the CO_2 concentration from 13 to 50 vol%, the mass transfer coefficient decreased linearly from 4.2 to 2.3 × 10^{-4} m/s (Fig. 8B), determining a 45% overall decreased. Furthermore, even though a slightly different slope was observed for CO_2 content > 30 vol%, no clear plateau was identified for the CO_2 flux (Fig. 8A) from the gas to the liquid phase, which increased monotonically from 6.4 to 17.0 mol/(m^2h) within the investigated range of feed gas compositions.

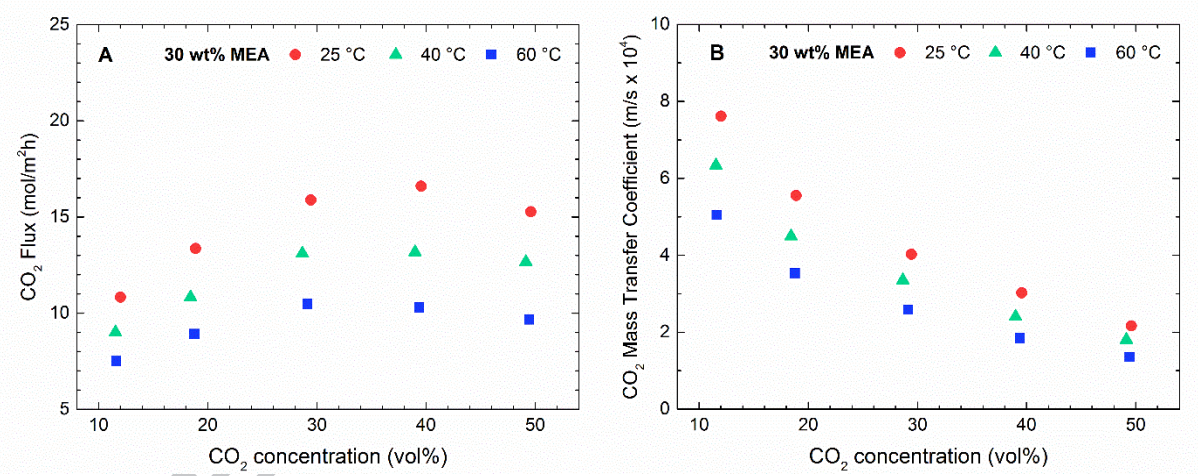

Figure 7 – Effect of CO_2 concentration in the feed gas on the measured CO_2 flux (A) and on the calculated overall mass transfer coefficient (B), when 30 wt% MEA is used as liquid phase. Operating conditions: liquid flow rate = 50 ml/min; gas flow rate = 250 ml/min; upstream pressure ≈ 1.1 bar.

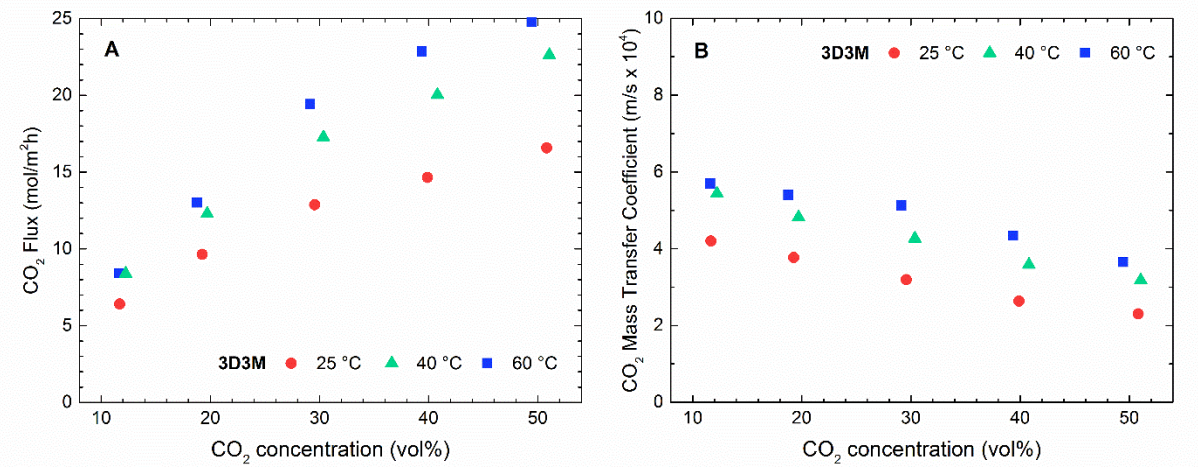

Figure 8 – Effect of CO_2 concentration in the feed gas on the measured CO_2 flux (A) and on the calculated overall mass transfer coefficient (B), when 3D3M is used as liquid phase. Operating conditions: liquid flow rate = 50 ml/min; gas flow rate = 250 ml/min; upstream pressure ≈ 1.1 bar.

Similar to the results at 13 vol% CO_2, the mass transport increased with temperature at all CO_2 concentrations as shown in Fig. 8A. The lower liquid viscosity at higher temperature is identified as the main reason for the observed trend. At room temperature, the differences between the 3D3M absorbent and the benchmark became smaller by increasing the CO_2 content in the feed gas, achieving similar results at 50 vol% CO_2 as seen when Fig.7A and Fig. 8A are compared. Interestingly, at temperature higher than 40 °C and CO_2 content > 20 vol%, the performance of 3D3M appeared to be systematically higher compared to 30 wt% MEA. The results proved that at high CO_2 content the liquid phase plays a major role in the determination of the CO_2 transport in the membrane contactor and changes in solvent properties like faster kinetics, can lead to higher CO_2 capture performance.

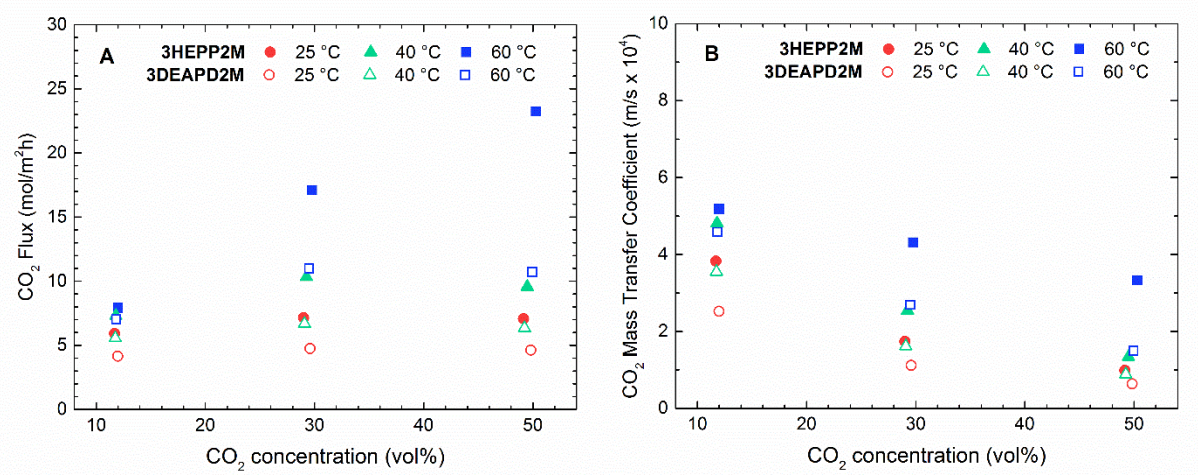

Figure 9 – Effect of CO_2 concentration in the feed gas on the measured CO_2 flux (A) and on the calculated overall mass transfer coefficient (B), when 3HEPP2M or 3DEAPD2M are used as liquid phase. Operating conditions: liquid flow rate = 50 ml/min; gas flow rate = 250 ml/min; upstream pressure ≈ 1.1 bar.

Figure 9 shows the results obtained for the other two investigated absorbents, 3HEPP2M and 3DEAPD2M. Similar to the previous cases, the mass transfer coefficient decreased at higher CO_2 content in the feed gas, with 75% drop at 50 vol% CO_2 for both absorbents (Fig. 9B). In terms of flux, a lower performance was observed compared to 3D3M, possibly due to

the higher viscosity: at 13 vol% and room temperature, the measured flux corresponded to 5.9 and 4.2 mol/(m^2h) for 3HEPP2M and 3DEAPD2M, respectively. Furthermore, similar to the MEA case, no significant differences were observed between the performance measured at 30 and 50 vol% CO_2: the flux stabilized at 7.1 and 4.7 mol/(m^2h) for 3HEPP2M and 3DEAPD2M, respectively. At higher temperature, the trends of the mass transfer coefficient and flux are similar to the ones observed at room temperature. However, 3HEPP2M at 60 °C performed similarly to that of 3D3M. In this case, the mass transfer flux increased with increasing CO_2 content in the feed gas reaching a value of 23.2 mol/(m^2h) at 50 vol% CO_2.

4.3.3 Effect of liquid flow

According to the results showed in the previous paragraphs, for the new amine blends the mass transfer resistance was found mainly located in the liquid phase, or more precisely, at the boundary layer of the liquid phase, the influence of the liquid flow rate was investigated. As shown in Fig.10, in the case of 30 wt% MEA, the liquid flow rate did not display significant differences. Within the investigated temperature range, an increase of the liquid flow rate from 50 to 150 ml/min resulted in negligible variation in the mass transfer coefficient. This confirms the previous assumption that when 30 wt% MEA is used as liquid phase, the membrane is mainly contributing to the mass transfer resistance.

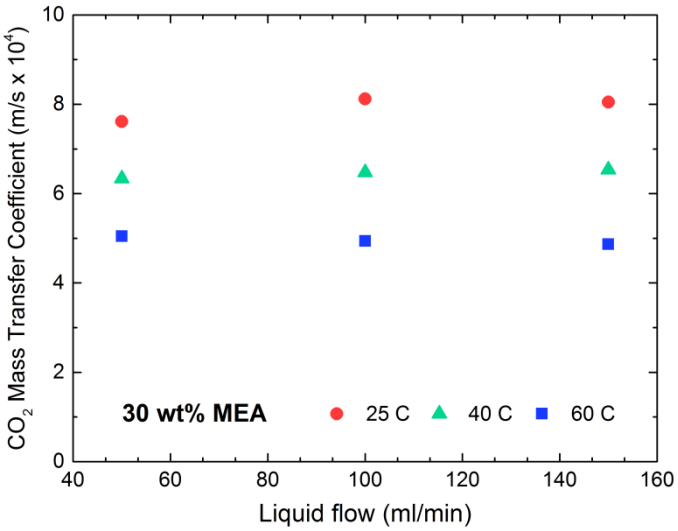

Figure 10 – Effect of liquid flow rate on the overall mass transfer coefficient measured from the membrane contactor tests when 30 wt% MEA is used as liquid phase. Operating conditions: CO_2 content in the feed gas = 13 vol% (balance N_2); gas flow rate = 250 ml/min; upstream pressure ≈ 1.1 bar.

Figure 11 shows the performance observed for the new amine blends at room temperature and 50 vol% CO_2 in the feed gas. The range of the liquid flow rate was limited within 50 and 100 ml/min to avoid membrane failures (the high viscosity generates a high liquid pressure inside the tubes due to the pumping effect, limiting the test of a higher liquid flow rates). For all the new absorbents, the mass transfer coefficient slowly increases along with the liquid flow rate. In the case of 3D3M, the mass transfer increased from 2.3 to 2.7× 10^{-4} m/s in the investigated range, corresponding to an overall increase of only 16%. Similar trends can be observed for 3HEPP2M and 3DEAPD2M. Although at high CO_2 content the liquid phase is supposed to be the main resistance of the system, the influence of the liquid flow rate is surprisingly rather limited, at least within the investigated liquid flow range. Similar tests were performed at higher temperature (40 and 60 °C), but the influence of the liquid flow rate on the overall mass transfer appeared to be even lower compared to the one observed at room temperature (at 40 °C: enhancement between 7 and 20%; at 60 °C: enhancement below 5%).

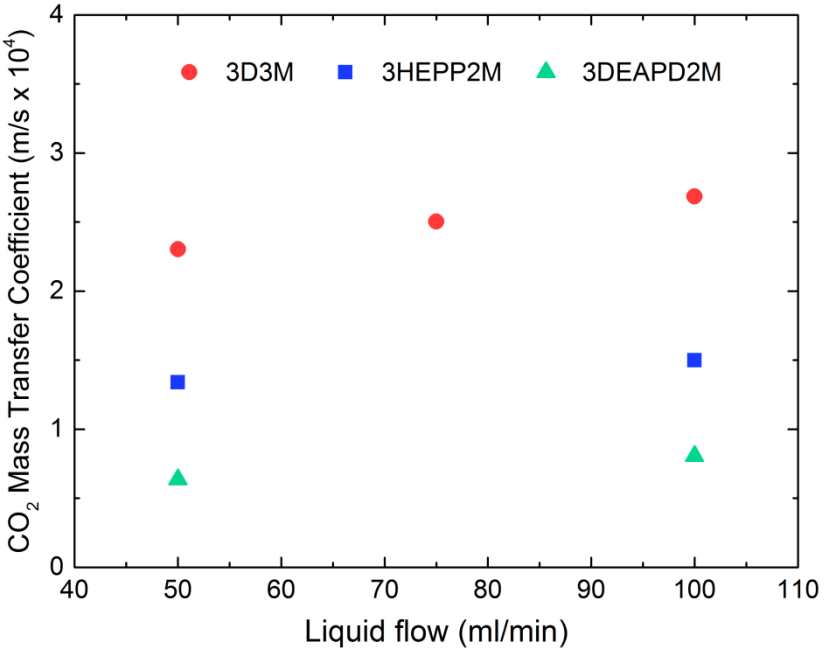

Figure 11 – Effect of liquid flow rate on the overall mass transfer coefficient measured from the membrane contactor tests using new amine blends. Operating conditions: CO_2 content in the feed gas = 50 vol% (balance N_2); temperature ≈ 25 °C, gas flow rate = 250 ml/min; upstream pressure ≈ 1.1 bar.

3.4. Mass transfer modelling

The experimental results are also compared with the K_{ov} values obtained from the resistance in series model (Eq. 3). Figure 12 shows the results obtained for the thin composite membrane when 30 wt% MEA was used. As shown in Fig. 12A, the resistance in series model offers a good approximation of the experimental values: when the average thickness is considered (1.7 µm), deviations below 10 % are observed in the low temperature range (T < 40 °C), while a larger error (24%) is detected at 60 °C. Nevertheless, the thickness of the dense layer affects the prediction to a notable extent. Varying this value within the interval of confidence estimated from the analysis of the SEM analysis (± 0.3 µm), the estimated overall mass transfer coefficient changes significantly (dotted lines in Fig. 13A). Extracting the contribution of each single phase to the overall resistance (Fig. 12B), it is clear that the membrane phase has the main share, being almost one order of magnitude larger than the gas and the liquid phase. These results again confirm the assumption that

the membrane is the main mass transfer resistance when 30 wt% MEA is used as liquid absorbent.

The good prediction offered by the model also supports the assumption that the mass transport in the liquid phase is not limited by the amine concentration at the membrane/liquid interface, despite the relatively high CO_2 partial pressure (13 kPa) in the feed gas. However, the model is not able to describe the decreased mass transfer coefficient at higher CO_2 concentrations (Fig. 7). Possibly, the higher CO_2 driving force consumes the amines present at the liquid boundary layer to a faster extent, so that the availability of reactive species becomes a limiting factor at the liquid/membrane interface. In addition, the assumption of a constant amine concentration at the liquid boundary layer is not valid anymore, so that the first order reaction kinetic assumption does not apply for these cases.

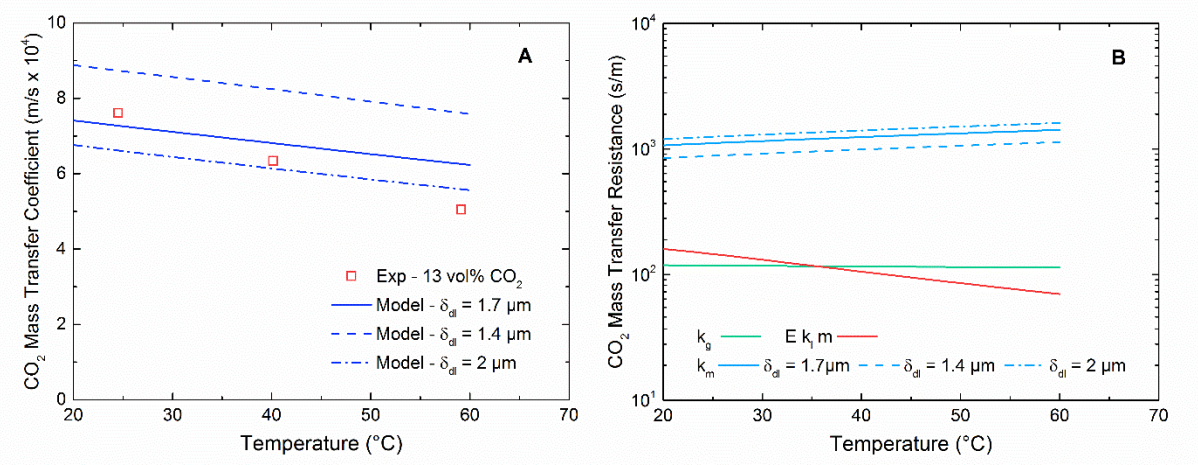

Figure 12 – Comparison of experimental results and modelling prediction (A) and contribution of the different phases to the overall mass transfer resistance (B) when 30 wt% MEA is used as liquid absorbent.

In the case of 3D3M, the model offers similar behavior as that of 30 wt% MEA (Figure 13). The model (green line, Fig. 13A) showed a mass transport that decreases with temperature, since the membrane remains the main contribution to the overall resistance, as reported in Fig. 13B. However, the experimental data showed that more CO_2 is absorbed at higher temperatures. In this view, the high viscosity characterizing the amine blends at low

temperature can represent a barrier to the availability of new reactive moieties at the interface, making the first order reaction kinetics (i.e., the amine concentration at the membrane/liquid interface does not limit the mass transfer) not valid anymore.

By means of a 2D model, Comite et al. [44] already showed that the boundary layer at the membrane/liquid boundary layer can have a significant influence on the mass transfer coefficient of porous membrane contactor. In the present case, to limit the model complexity, the effect is accounted by adding an additional term to the overall resistance, so that Eq. 3 becomes:

$$\frac{1}{K_{ov}} = \frac{1}{k_g} + \frac{1}{k_m} + \frac{1}{k_{lbl}} + \frac{1}{m\,E\,k_l} \tag{6}$$

where k_{lbl} is the mass transfer coefficient of the liquid boundary layer at the membrane interface directly in contact with the dense coating. Assuming a fast reactivity of the solvent, this liquid film is characterized by a complete saturation of the CO_2 reactive moieties. Therefore, CO_2 molecules can only be physically absorbed and need to diffuse to the bulk liquid to be able to react with basic moieties. The permeability of this boundary layer can be described according to the solution diffusion model, as product of the Henry's constant and the diffusion coefficient calculated for the saturated solvent. Hence, k_{lbl} can be calculated as:

$$\frac{1}{k_{lbl}} = \frac{\delta_{lbl}\,v_m}{P_{lbl}\,R\,T} \tag{7}$$

where δ_{lbl} is the thickness. P_{lbl} is the permeability of the liquid boundary layer and can be evaluated as follows [45]:

$$P_{lbl} = m\ D_{CO_2,\,sat} \tag{8}$$

where m is the partitioning coefficient for the physical CO_2 absorption estimated from N_2O solubility experiments [6] and $D_{CO_2,\,sat}$ is the diffusion coefficient of CO_2 calculated with the

Stokes-Einstein equation (see Appendix) using the liquid absorbent viscosity measured for the saturated solvents (Table S1).

Under these assumptions, the only adjustable parameter is the thickness of the liquid boundary layer, and by assuming a 150 nm thick boundary layer in contact with the membrane phase, a rather good prediction of the data is obtained (red line, Fig. 13A). The effect of this boundary layer is reduced at higher temperature due to the significant decrease of viscosity, producing a larger CO_2 diffusion coefficient. Analyzing the different resistances to the mass transfer (Fig. 13B), it is clear how the contribution of the liquid boundary layer is significant in the low temperature range, where the absorbent viscosity is quite high. At temperature higher than 40 °C, the membrane phase dominates again the mass transport and the model's prediction becomes similar to the one obtained under the assumption of pseudo-first order reaction kinetics.

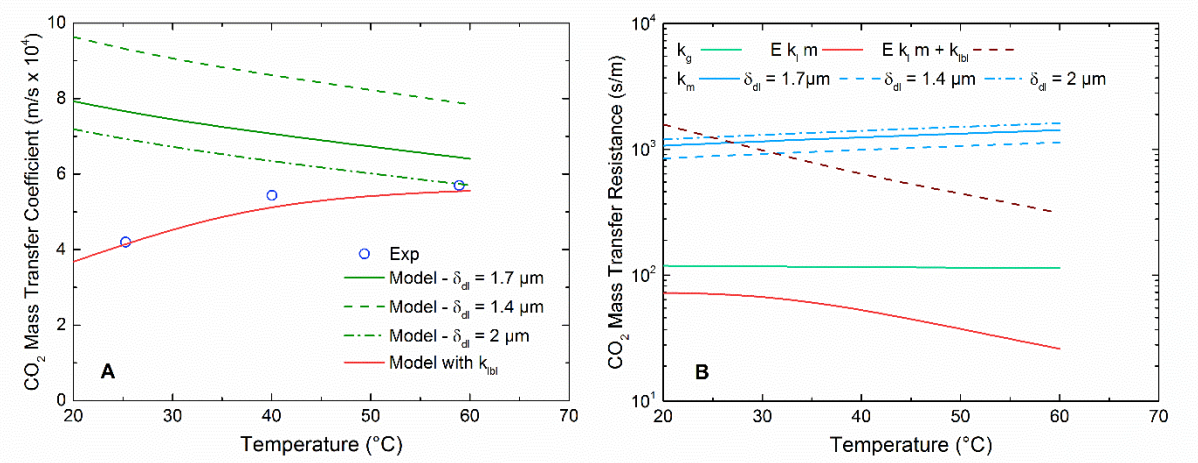

Figure 13 – Comparison of experimental results and modelling prediction (A) and contribution of the different phases to the overall mass transfer resistance (B) when 3D3M is used as liquid absorbent.

In the case of the other amine blends (i.e., 3HEPP2M and 3DEAPD2M) tested in the present investigation, no data are available to allow a modelling analysis of the achieved results. However, it is interesting to notice (Table S1) that upon CO_2 loading, a similar increase of viscosity is observed, possibly explaining the similar trends observed experimentally.

Despite its empirical nature, the proposed model interpretation clearly suggests that for viscous absorbents the establishment of a liquid boundary layer can significantly affect the transport. In particular, the limitation comes apparently from the diffusion of reactive species towards the membrane/liquid interface rather than from the CO_2 diffusion away from the dense coating surface. The appearance of this effect seems to be more severe at increasing the solvent viscosity. To accurately predict the experimental data, a more complex 2D model should be used to this purpose and it will be considered in our further work.

5. Conclusions

In the present work, the CO_2 capture performances of new amine blends, with promising features in terms of cyclic capacity and regeneration energy requirements, have been investigated in a non-porous membrane contactor setup.

Despite the higher performance expected at room temperature, the mass transfer coefficient measured for the new amine blends in the membrane contactor is found to be 50% lower compared to the benchmark (30 wt% MEA). The much higher viscosity has been identified as the possible cause of the reduced capture performance of the new absorbents. An increase in operating temperature to 40 and 60 °C narrowed the differences between the mass transfer coefficients of the amine blends and the benchmark, possibly due to the sharp reduction in viscosity. Interestingly, for CO_2 amounts larger than 20 vol% CO_2 and temperature higher than ambient conditions, the 3D3M solvent showed systematically improved performance compared to the benchmark, highlighting a promising potential for capture applications with relatively high CO_2 content (e.g., biogas upgrading).

The resistance in series model is observed to provide a good agreement for the modelling of

the benchmark, but it could not provide a suitable representation in the case of the amine blend (3D3M). This is possibly related to the underestimation of the effect of the liquid boundary layer. A modified model is proposed, showing that a fast saturation of 140 nm of the liquid layer on the top of the dense membrane could be already responsible for the lower efficiency observed experimentally at low temperature.

The present investigation set the base for the optimization of membrane contactor system exploiting absorbents with performance closer to the industrial goal. It was clearly shown that, at low temperature, the use of absorbents with faster kinetics and higher loading capacity did not lead to a higher membrane contactor performance compared to the benchmark. However, a promising potential is obtained for more concentrated gaseous streams. Future works will focus on development of 2D model to better describe the liquid boundary layer and on the assessment of hollow fiber membrane contactor performance.

Appendix

For the gas side, the mass transfer coefficient reported in Eq. 3 is calculated according to a Sherwood number correlation [46], as suggested by other authors for similar configuration [47,48]:

$$k_g = \frac{D_{CO_2,g}}{d_h} \cdot 0.023 \cdot Re^{0.8} \cdot Sc^{0.33} \quad (9)$$

where $D_{CO_2,g}$ is the CO_2 diffusivity in the gas phase (calculated according to Fuller correlation [49]), d_h is the hydraulic diameter and Re and Sc are the Reynolds and Schmidt numbers, respectively.

Concerning the liquid phase, the mass transfer resistance is estimated assuming a pseudo-first order reaction kinetics, where the diffusion of the reactive species within the liquid layer is not limiting the reaction. Under this assumption, the enhancement factor can be

approximated to the Hatta number [50], and $E\,k_l$ can be calculated according to intrinsic properties of the liquid absorbents:

$$E\,k_l = \sqrt{D_{CO_2,abs} k_{obs}} \quad (10)$$

where $D_{CO_2,l}$ is the CO_2 diffusivity in the liquid absorbent and k_{obs} is the first order rate constant. $D_{CO_2,l}$ is the CO_2 diffusivity in the liquid absorbent and is estimated using a modified Stoke-Einstein equation [51]:

$$D_{CO_2,l} = D_{CO_2,w}\left(\frac{\mu_w}{\mu_l}\right)^{0.6} \quad (11)$$

where $D_{CO_2,w}$ is the diffusion coefficient of CO_2 in water [51], and μ_w and μ_l are the viscosities of water and the liquid absorbent, respectively.

In the case of 30 wt% MEA, k_{obs} and the partitioning coefficient m are calculated according to the data provided by Luo et al. [52]. In the case of DEEA-MAPA blends, literature values are reported by Monteiro et al. [6]. However, no data for the exact blend 3D3M is reported. Therefore, k_{obs} and m reported for a 3M DEEA 2M MAPA solution were assumed valid also for 3D3M, being the closest approximation of the liquid absorbent used in this work. In the case of m, this assumption was supported by the fact that a deviation smaller than 5% was observed between the data obtained for 3M DEEA 2M MAPA and 3M DEEA 1M MAPA. For the other blends tested no literature data for k_{obs} and of the partitioning coefficient m was found.

Acknowledgement

The authors would like to thank Vanja Buvik for performing the TOC analyses and Prof. Hallvard Svendsen for the fruitful discussions.

Funding

This work was supported by the Research Council of Norway (CLIMIT: New concepts for CO_2 capture, Project No. 239789)

References

[1] J. Rogelj, M. den Elzen, N. Höhne, T. Fransen, H. Fekete, H. Winkler, R. Schaeffer, F. Sha, K. Riahi, M. Meinshausen, Paris Agreement climate proposals need a boost to keep warming well below 2 °C, Nature. 534 (2016) 631. http://dx.doi.org/10.1038/nature18307.

[2] S.I. Seneviratne, M.G. Donat, A.J. Pitman, R. Knutti, R.L. Wilby, Allowable CO2 emissions based on regional and impact-related climate targets, Nature. 529 (2016) 477. http://dx.doi.org/10.1038/nature16542.

[3] J. Huang, H. Yu, A. Dai, Y. Wei, L. Kang, Drylands face potential threat under 2 °C global warming target, Nat. Clim. Chang. 7 (2017) 417. http://dx.doi.org/10.1038/nclimate3275.

[4] P.H.M. Feron, Introduction, in: Absorption-Based Post-Combustion Capture of Carbon Dioxide, Elsevier, 2016: pp. 3–12. doi:10.1016/B978-0-08-100514-9.00001-9.

[5] A. V Rayer, P.D. Mobley, M. Soukri, T.R. Gohndrone, J. Tanthana, J. Zhou, M. Lail, Absorption rates of carbon dioxide in amines in hydrophilic and hydrophobic solvents, Chem. Eng. J. 348 (2018) 514–525. doi:10.1016/j.cej.2018.03.193.

[6] J.G.M.S. Monteiro, H. Majeed, H. Knuutila, H.F. Svendsen, Kinetics of CO2 absorption in aqueous blends of N,N-diethylethanolamine (DEEA) and N-methyl-1,3-propane-diamine (MAPA), Chem. Eng. Sci. 129 (2015) 145–155. doi:http://dx.doi.org/10.1016/j.ces.2015.02.001.

[7] G. Rochelle, E. Chen, S. Freeman, D. Van Wagener, Q. Xu, A. Voice, Aqueous piperazine as the new standard for CO2 capture technology, Chem. Eng. J. 171 (2011) 725–733. doi:https://doi.org/10.1016/j.cej.2011.02.011.

[8] I.M. Bernhardsen, H.K. Knuutila, A review of potential amine solvents for CO2 absorption

process: Absorption capacity, cyclic capacity and pKa, Int. J. Greenh. Gas Control. 61 (2017) 27–48. doi:10.1016/J.IJGGC.2017.03.021.

[9] Z. Liang, K. Fu, R. Idem, P. Tontiwachwuthikul, Review on current advances, future challenges and consideration issues for post-combustion CO2 capture using amine-based absorbents, Chinese J. Chem. Eng. 24 (2016) 278–288. doi:10.1016/J.CJCHE.2015.06.013.

[10] Y. Du, Y. Yuan, G.T. Rochelle, Capacity and absorption rate of tertiary and hindered amines blended with piperazine for CO2 capture, Chem. Eng. Sci. 155 (2016) 397–404. doi:10.1016/J.CES.2016.08.017.

[11] L. Wang, S. An, Q. Li, S. Yu, S. Wu, Phase change behavior and kinetics of CO2 absorption into DMBA/DEEA solution in a wetted-wall column, Chem. Eng. J. 314 (2017) 681–687. doi:https://doi.org/10.1016/j.cej.2016.12.033.

[12] D.D.D. Pinto, H. Knuutila, G. Fytianos, G. Haugen, T. Mejdell, H.F. Svendsen, CO2 post combustion capture with a phase change solvent. Pilot plant campaign, Int. J. Greenh. Gas Control. 31 (2014) 153–164. doi:http://dx.doi.org/10.1016/j.ijggc.2014.10.007.

[13] H.K. Knuutila, Å. Nannestad, Effect of the concentration of MAPA on the heat of absorption of CO2 and on the cyclic capacity in DEEA-MAPA blends, Int. J. Greenh. Gas Control. 61 (2017) 94–103. doi:10.1016/J.IJGGC.2017.03.026.

[14] C. Perinu, I.M. Bernhardsen, D.D.D. Pinto, H.K. Knuutila, K.-J. Jens, NMR Speciation of Aqueous MAPA, Tertiary Amines, and Their Blends in the Presence of CO2: Influence of pKa and Reaction Mechanisms, Ind. Eng. Chem. Res. 57 (2018) 1337–1349. doi:10.1021/acs.iecr.7b03795.

[15] H.K. Knuutila, R. Rennemo, A.F. Ciftja, New solvent blends for post-combustion CO2 capture: Screening and VLE performance, Green Energy Environ. submitted (2018).

[16] A. Hartono, F. Saleem, M.W. Arshad, M. Usman, H.F. Svendsen, Binary and ternary VLE of the 2-(diethylamino)-ethanol (DEEA)/3-(methylamino)-propylamine (MAPA)/water system, Chem. Eng. Sci. 101 (2013) 401–411. doi:http://dx.doi.org/10.1016/j.ces.2013.06.052.

[17] X. Chen, G. Huang, C. An, Y. Yao, S. Zhao, Emerging N-nitrosamines and N-nitramines from amine-based post-combustion CO2 capture – A review, Chem. Eng. J. 335 (2018) 921–935. doi:https://doi.org/10.1016/j.cej.2017.11.032.

[18] L. Ansaloni, A. Arif, A.F. Ciftja, H.K. Knuutila, L. Deng, Development of Membrane Contactors Using Phase Change Solvents for CO2 Capture: Material Compatibility Study, Ind. Eng. Chem. Res. 55 (2016) 13102–13113. doi:10.1021/acs.iecr.6b03901.

[19] L. Ansaloni, R. Rennemo, H.K. Knuutila, L. Deng, Development of membrane contactors using volatile amine-based absorbents for CO2capture: Amine permeation through the membrane, J. Memb. Sci. 537 (2017) 272–282. doi:10.1016/j.memsci.2017.05.016.

[20] S. Zhao, P.H.M. Feron, L. Deng, E. Favre, E. Chabanon, S. Yan, J. Hou, V. Chen, H. Qi, Status and progress of membrane contactors in post-combustion carbon capture: A state-of-the-art review of new developments, J. Memb. Sci. 511 (2016) 180–206. doi:http://dx.doi.org/10.1016/j.memsci.2016.03.051.

[21] D. deMontigny, P. Tontiwachwuthikul, A. Chakma, Comparing the Absorption Performance of Packed Columns and Membrane Contactors, Ind. Eng. Chem. Res. 44 (2005) 5726–5732. doi:10.1021/ie040264k.

[22] P.J. Gusnawan, S. Zha, L. Zou, G. Zhang, J. Yu, Soybean and moringa based green biosolvents for low-concentration CO2 capture via a hollow fiber membrane contactor, Chem. Eng. J. 335 (2018) 631–637. doi:https://doi.org/10.1016/j.cej.2017.11.023.

[23] M.R. DashtArzhandi, A.F. Ismail, T. Matsuura, B.C. Ng, M.S. Abdullah, Fabrication and characterization of porous polyetherimide/montmorillonite hollow fiber mixed matrix membranes for CO2 absorption via membrane contactor, Chem. Eng. J. 269 (2015) 51–59. doi:https://doi.org/10.1016/j.cej.2015.01.095.

[24] Y.-F. Lin, Q. Ye, S.-H. Hsu, T.-W. Chung, Reusable fluorocarbon-modified electrospun PDMS/PVDF nanofibrous membranes with excellent CO2 absorption performance, Chem. Eng. J. 284 (2016) 888–895. doi:https://doi.org/10.1016/j.cej.2015.09.063.

[25] C.A. Scholes, M. Simioni, A. Qader, G.W. Stevens, S.E. Kentish, Membrane gas–solvent contactor trials of CO2 absorption from syngas, Chem. Eng. J. 195–196 (2012) 188–197. doi:https://doi.org/10.1016/j.cej.2012.04.034.

[26] P.T. Nguyen, E. Lasseuguette, Y. Medina-Gonzalez, J.C. Remigy, D. Roizard, E. Favre, A dense membrane contactor for intensified CO2 gas/liquid absorption in post-combustion capture, J. Memb. Sci. 377 (2011) 261–272. doi:http://dx.doi.org/10.1016/j.memsci.2011.05.003.

[27] E. Favre, H.F. Svendsen, Membrane contactors for intensified post-combustion carbon dioxide capture by gas–liquid absorption processes, J. Memb. Sci. 407–408 (2012) 1–7. doi:http://dx.doi.org/10.1016/j.memsci.2012.03.019.

[28] B. Ozturk, R. Hughes, Evaluation of mass transfer characteristics of non-porous and microporous membrane contactors for the removal of CO2, Chem. Eng. J. 195–196 (2012) 122–131. doi:https://doi.org/10.1016/j.cej.2012.04.085.

[29] C.A. Scholes, S.E. Kentish, G.W. Stevens, D. deMontigny, Comparison of thin film composite and microporous membrane contactors for CO2 absorption into monoethanolamine, Int. J. Greenh. Gas Control. 42 (2015) 66–74. doi:http://dx.doi.org/10.1016/j.ijggc.2015.07.032.

[30] E. Chabanon, D. Roizard, E. Favre, Membrane Contactors for Postcombustion Carbon Dioxide Capture: A Comparative Study of Wetting Resistance on Long Time Scales, Ind. Eng. Chem. Res. 50 (2011) 8237–8244. doi:10.1021/ie200704h.

[31] Z. Dai, L. Ansaloni, L. Deng, Precombustion CO<inf>2</inf> Capture in Polymeric Hollow Fiber Membrane Contactors Using Ionic Liquids: Porous Membrane versus Nonporous Composite Membrane, Ind. Eng. Chem. Res. 55 (2016). doi:10.1021/acs.iecr.6b01247.

[32] C.A. Scholes, S.E. Kentish, G.W. Stevens, J. Jin, D. deMontigny, Thin-film composite membrane contactors for desorption of CO2 from Monoethanolamine at elevated temperatures, Sep. Purif. Technol. 156, Part (2015) 841–847. doi:http://dx.doi.org/10.1016/j.seppur.2015.11.010.

[33] S. Bazhenov, A. Malakhov, D. Bakhtin, V. Khotimskiy, G. Bondarenko, V. Volkov, M. Ramdin,

T.J.H. Vlugt, A. Volkov, CO2 stripping from ionic liquid at elevated pressures in gas-liquid membrane contactor, Int. J. Greenh. Gas Control. 71 (2018) 293–302. doi:https://doi.org/10.1016/j.ijggc.2018.03.001.

[34] C.A. Scholes, A. Qader, G.W. Stevens, S.E. Kentish, Membrane Gas-Solvent Contactor Pilot Plant Trials of CO2 Absorption from Flue Gas, Sep. Sci. Technol. 49 (2014) 2449–2458. doi:10.1080/01496395.2014.937499.

[35] E. Chabanon, E. Kimball, E. Favre, O. Lorain, E. Goetheer, D. Ferre, A. Gomez, P. Broutin, Hollow Fiber Membrane Contactors for Post-Combustion CO2 Capture: A Scale-Up Study from Laboratory to Pilot Plant, Oil Gas Sci. Technol. – Rev. IFP Energies Nouv. 69 (2014) 1035–1045. http://dx.doi.org/10.2516/ogst/2012046.

[36] Z. Dai, L. Ansaloni, J.J. Ryan, R.J. Spontak, L. Deng, Nafion/IL hybrid membranes with tuned nanostructure for enhanced CO<inf>2</inf>separation: Effects of ionic liquid and water vapor, Green Chem. 20 (2018). doi:10.1039/C7GC03727A.

[37] M. Saeed, L. Deng, Post-combustion CO2 membrane absorption promoted by mimic enzyme, J. Memb. Sci. 499 (2016) 36–46. doi:10.1016/J.MEMSCI.2015.10.014.

[38] S.B. Iversen, V.K. Bhatia, K. Dam-Johansen, G. Jonsson, Characterization of microporous membranes for use in membrane contactors, J. Memb. Sci. 130 (1997) 205–217. doi:https://doi.org/10.1016/S0376-7388(97)00026-4.

[39] J. Zhang, P.S. Fennell, J.P.M. Trusler, Density and Viscosity of Partially Carbonated Aqueous Tertiary Alkanolamine Solutions at Temperatures between (298.15 and 353.15) K, J. Chem. Eng. Data. 60 (2015) 2392–2399. doi:10.1021/acs.jced.5b00282.

[40] G. Firpo, E. Angeli, L. Repetto, U. Valbusa, Permeability thickness dependence of polydimethylsiloxane (PDMS) membranes, J. Memb. Sci. 481 (2015) 1–8. doi:https://doi.org/10.1016/j.memsci.2014.12.043.

[41] Z. Cui, D. deMontigny, Part 7: A review of CO2 capture using hollow fiber membrane contactors, Carbon Manag. 4 (2013) 69–89. doi:10.4155/cmt.12.73.

[42] J. Franco, D. deMontigny, S. Kentish, J. Perera, G. Stevens, A Study of the Mass Transfer of CO2 through Different Membrane Materials in the Membrane Gas Absorption Process, Sep. Sci. Technol. 43 (2008) 225–244. doi:10.1080/01496390701791554.

[43] H. Kreulen, C.A. Smolders, G.F. Versteeg, W.P.M. van Swaaij, Microporous hollow fibre membrane modules as gas-liquid contactors. Part 1. Physical mass transfer processes: A specific application: Mass transfer in highly viscous liquids, J. Memb. Sci. 78 (1993) 197–216. doi:https://doi.org/10.1016/0376-7388(93)80001-E.

[44] A. Comite, C. Costa, M. Demartini, R. Di Felice, M. Rotondi, Rate of CO2 transfer to loaded MEA solutions using a membrane contactor device, Int. J. Greenh. Gas Control. 52 (2016) 378–386. doi:https://doi.org/10.1016/j.ijggc.2016.07.029.

[45] H. Yasuda, Units of gas permeability constants, J. Appl. Polym. Sci. 19 (1975) 2529–2536. doi:10.1002/app.1975.070190915.

[46] E.R. Gilliland, T.K. Sherwood, Diffusion of Vapors into Air Streams, Ind. Eng. Chem. 26 (1934) 516–523. doi:10.1021/ie50293a010.

[47] F. Bougie, I. Iliuta, M.C. Iliuta, Flat sheet membrane contactor (FSMC) for CO2 separation using aqueous amine solutions, Chem. Eng. Sci. 123 (2015) 255–264. doi:https://doi.org/10.1016/j.ces.2014.10.041.

[48] S.-H. Lin, K.-L. Tung, H.-W. Chang, K.-R. Lee, Influence of fluorocarbon flat-membrane hydrophobicity on carbon dioxide recovery, Chemosphere. 75 (2009) 1410–1416. doi:https://doi.org/10.1016/j.chemosphere.2009.02.027.

[49] E.N. Fuller, P.D. Schettler, J.C. Giddings, New method for prediction of binary gas-phase diffusion coefficients, Ind. Eng. Chem. 58 (1966) 18–27. doi:10.1021/ie50677a007.

[50] W.P.M. van Swaaij, G.F. Versteeg, Mass transfer accompanied with complex reversible chemical reactions in gas—liquid systems: an overview, Chem. Eng. Sci. 47 (1992) 3181–3195. doi:https://doi.org/10.1016/0009-2509(92)85028-A.

[51] G.F. Versteeg, W.P.M. Van Swaaij, Solubility and diffusivity of acid gases (carbon dioxide,

nitrous oxide) in aqueous alkanolamine solutions, J. Chem. Eng. Data. 33 (1988) 29–34. doi:10.1021/je00051a011.

[52] X. Luo, A. Hartono, S. Hussain, H.F. Svendsen, Mass transfer and kinetics of carbon dioxide absorption into loaded aqueous monoethanolamine solutions, Chem. Eng. Sci. 123 (2015) 57–69. doi:https://doi.org/10.1016/j.ces.2014.10.013.

Highlights

- CO_2 capture in non-porous membrane contactors using new amine solvents was evaluated.
- Solvent viscosity significantly affects the performance of the system.
- The mass transfer coefficient decreases with at higher CO_2 content in the feed gas.
- Liquid flow rate has limited impact on the membrane contactor performance.
- The liquid boundary layer resistance is significant for highly viscous absorbents.

Graphical Abstract